

Quantum many-body simulation using monolayer exciton-polaritons in coupled-cavities

Hai-Xiao Wang,¹ Alan Zhan,² Ya-Dong Xu,¹ Huan-Yang Chen,¹
Wen-Long You,^{1,*} Arka Majumdar,^{2,3,†} and Jian-Hua Jiang^{1,‡}

¹*College of Physics, Optoelectronics and Energy,*

& Collaborative Innovation Center of Suzhou Nano Science and Technology,

Soochow University, 1 Shizi Street, Suzhou 215006, China

²*Department of Physics, University of Washington, Seattle, Washington 98195, USA*

³*Department of Electrical Engineering,*

University of Washington, Seattle, Washington 98195, USA

(Dated: April 20, 2017)

Abstract

Quantum simulation is a promising approach to understand complex strongly correlated many-body systems using relatively simple and tractable systems. Photon-based quantum simulators have great advantages due to the possibility of direct measurements of multi-particle correlations and ease of simulating non-equilibrium physics. However, interparticle interaction in existing photonic systems is often too weak limiting the potential of quantum simulation. Here we propose an approach to enhance the interparticle interaction using exciton-polaritons in MoS₂ monolayer quantum-dots embedded in 2D photonic crystal microcavities. Realistic calculation yields optimal repulsive interaction in the range of 1-10 meV — more than an order of magnitude greater than the state-of-art value. Such strong repulsive interaction is found to emerge neither in the photon-blockade regime for small quantum dot nor in the polariton-blockade regime for large quantum dot, but in the crossover between the two regimes with a moderate quantum-dot radius around 20 nm. The optimal repulsive interaction is found to be largest in MoS₂ among commonly used optoelectronic materials. Quantum simulation of strongly correlated many-body systems in a finite chain of coupled cavities and its experimental signature are studied via exact diagonalization of the many-body Hamiltonian. A method to simulate 1D superlattices for interacting exciton-polariton gases in serially coupled cavities is also proposed. Realistic considerations on experimental realizations reveal advantages of transition metal dichalcogenide monolayer quantum-dots over conventional semiconductor quantum-emitters.

* wlyou@suda.edu.cn

† arka@uw.edu

‡ jianhuajiang@suda.edu.cn

I. INTRODUCTION

Solving strongly correlated quantum many-body systems exactly is a formidable task. One promising approach is to mimic such complicated systems using another simpler and easily controllable quantum system, as envisioned by Feynman[1]. To that end, the first demonstration of quantum phase transition with ultracold atoms in an optical lattice sparked a large body of research on quantum simulation in ultracold atomic systems[2, 3]. Interacting photons also provide a unique and distinctive platform to study strongly correlated quantum many-body systems[4–8]. The main idea behind this approach is to create an interacting “quantum fluid of light” [9] via a coupled network of nonlinear photonic cavities[4–11]. Advantages of photonic quantum simulators include much higher energy scale and faster operations, available non-destructive techniques for direct measurements of quasiparticle properties via spatial- and/or time-resolved multi-photon correlation functions, and abundant optical methods for coherent control[9, 12]. Such multi-particle correlation measurement is extremely difficult in both cold-atomic gases and strongly correlated electronic materials. These advantages yield great promises for photonic quantum many-body simulation as a way to understand the role of many-body quantum entanglement in Mott insulators which remains an outstanding challenge to fundamental physics[13].

Polariton, a quantum superposition of a photon and an exciton, emerges in hybrid strongly coupled systems of photonic microcavity and semiconductor excitons [11, 14]. The composite nature of polaritons leads to various unusual properties, such as high-temperature Bose-Einstein condensation (BEC)[14–17], and enhanced optical nonlinearity for applications in all-optical diodes[18] and transistors[19]. However, optical nonlinearity in those systems generally requires high polariton densities. Achieving optical nonlinearity at the single photon level requires significant reduction of the cavity mode-area/volume and optimization of the optoelectronic material (typically forming a semiconductor quantum dot)[20]. Note that, such single photon nonlinearity is necessary to realize the aforementioned photonic quantum simulators. Photon blockade, the effect where a single photon repels other photons, has been observed using a very small quantum dot (QD) coupled to a cavity[21–24]. In those systems, Pauli blockade forbids double-occupancy of excitons, hence the interaction between polaritons is simply given by the energy difference between free polaritons and the Pauli blockade polaritons, i.e., $U_{pl} = (2 - \sqrt{2})\hbar\Omega$, where $\hbar\Omega$ denotes the exciton-photon

interaction strength[21–23]. However, the area of QD $\sim (10 \text{ nm})^2$, is much smaller than the modal area of the optical cavity, leading to much reduced light-matter interaction and polariton-polariton repulsion. The state-of-the-art value of polariton repulsive interaction in the photon-blockade regime is less than 0.1 meV[24]. Thus an important challenge for polariton quantum many-body simulation is to realize much stronger repulsive interaction.

In this work, we propose an optoelectronic architecture to realize polariton repulsion much larger than the state-of-the-art value, 1~10 meV, using exciton-polaritons based on monolayer MoS₂ QDs embedded in slab photonic crystal cavities. The strength of the repulsive interaction varies with the quantum dot radius due to the competition between the exciton-photon interaction and the exciton-exciton repulsion. It is found that the strongest repulsive interaction emerges neither in the photon-blockade regime for small QDs nor in the polariton-blockade regime for large QDs, but in the crossover between the two regimes. An optimal quantum dot radius is found as $\sim 20 \text{ nm}$. Similar trends are found for other common materials such as GaAs, InAs, CdTe, and GaN. Nevertheless, MoS₂ provides the largest nonlinearity, thanks to strong light-matter and exciton-exciton interactions. We further investigate possible experimental consequences of quantum simulation in a chain of coupled cavities using exact diagonalization of the many-body Hamiltonian. In addition, a method for simulation of superlattices in coupled cavities is proposed and the regimes for Mott transition is estimated using single- and two-particle analysis. Realistic considerations for fabrication and measurements reveal advantages of transition metal dichalcogenide (TMD) monolayer semiconductors over conventional optoelectronic materials.

II. MATERIAL AND PHOTONIC ARCHITECTURE

The proposed architecture is illustrated in Fig. 1(a). The cavity is formed by a point defect in a 2D hexagonal photonic crystal slab, also known as the H1 cavity [25] [see Supplementary Materials[26]]. The MoS₂ QD can be fabricated via patterning a MoS₂ monolayer and placed at the center of the cavity. A network of the cavity-QD hybrid structure forms an interacting polariton lattice system, which is described by the following Hamiltonian[9]

$$\mathcal{H} = \sum_i [\hbar\omega_c c_i^\dagger c_i + \hbar\omega_X b_i^\dagger b_i + \hbar\Omega(c_i b_i^\dagger + b_i c_i^\dagger) + \frac{1}{2}U_X \mathcal{N}_i(\mathcal{N}_i - 1)] - t \sum_{\langle i,j \rangle} c_i^\dagger c_j. \quad (1)$$

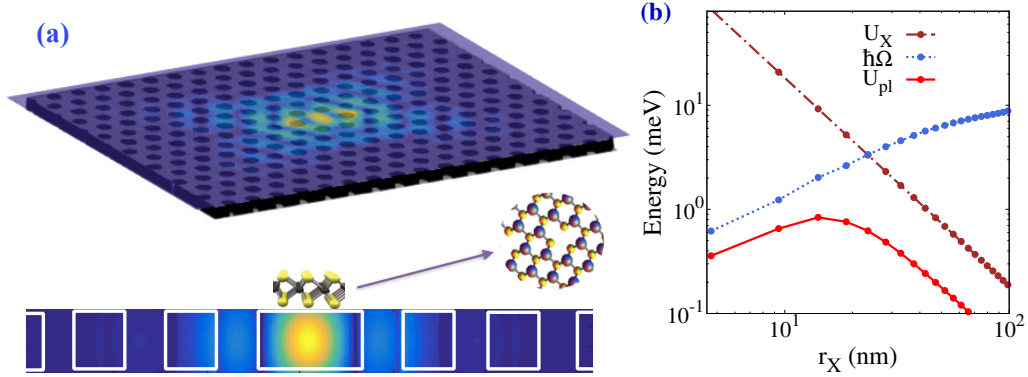


FIG. 1. (a) Cavity-QD hybrid system for strongly interacting polaritons. Upper panel: The H1 cavity will be realized using a thin 2D photonic crystal slab. A MoS₂ QD is placed at the center of the cavity. Lower panel: Inplane electric field distribution in the x - z plane (field outside the membrane is not plotted). The position of the MoS₂ QD is illustrated using a schematic of atomic structure of MoS₂. (b) Exciton-exciton interaction U_X , exciton-photon interaction $\hbar\Omega$, and polariton-polariton interaction U_{pl} as functions of the QD radius r_X for MoS₂ with zero detuning.

Here ω_c is the frequency of the cavity mode, c_i^\dagger (b_i^\dagger) creates a photon (exciton) in the i^{th} cavity (QD), $\mathcal{N}_i = b_i^\dagger b_i$ stands for the exciton number operator, U_X denotes the exciton-exciton repulsion, $\hbar\Omega$ represents the exciton-photon interaction, and $\hbar\omega_X = 1.87$ eV is the exciton energy in MoS₂ QDs. We assume that ω_c is identical for each cavity and ω_X is the same for each MoS₂ QD. The effects of fluctuation and disorder will be considered later. From Refs. [14, 17], the exciton-photon coupling is

$$\hbar\Omega = \frac{d_{cv}|\phi(0)|\sqrt{\hbar\omega_c}}{\sqrt{2\epsilon_0 L_c}}, \quad (2)$$

where $d_{cv} = 4.0 \times 10^{-29}$ C·m is the interband dipole matrix element[17, 27] and $|\phi(0)| = \sqrt{2/(\pi a_B^2)}$ is the exciton wave amplitude at zero electron-hole distance ($a_B = 1$ nm is the exciton Bohr radius in MoS₂[28]). The exciton-photon coupling depends on the following quantity of the dimension of length,

$$L_c \equiv \frac{\int_c d\vec{r} \epsilon(\vec{r}) |\vec{E}(\vec{r})|^2}{\int_c dx dy |\vec{E}(x, y, z_0)|^2 \Theta(x, y, z_0)}, \quad (3)$$

where $\epsilon(\vec{r})$ is the position-dependent (relative) dielectric constant, $\vec{E}(\vec{r})$ is the electric field of the cavity mode, and z_0 is the z coordinate of the MoS₂ monolayer. The $\Theta(x, y, z_0)$ function,

which takes into account the finite overlap between the QD and the cavity optical field, is unity in the QD region and zero outside[14]. The integrals are carried out within each cavity. The exciton-exciton interaction strength is given by[29] $U_X = \frac{6E_b a_B^2}{S_X}$, where $E_b = 0.96$ eV is the exciton binding energy and $S_X = \pi r_X^2$ is the area of the circular MoS₂ QD with radius r_X . The last term in Eq. (1) describes photon hopping between nearest-neighbor cavities, where t is the hopping energy. Note that in the above formalism, the exciton-polariton is approximately treated as uniformly distributed in the QDs [resulting in $\Theta(x)$ in Eq. (3) and the S_x factor in U_X]. More rigorous treatment with non-uniform distribution is equivalent to a correction of the effective area of the polariton, which affects the results marginally [see supplementary materials].

The designed H1 cavity has a slab thickness of 110 nm and a lattice periodicity of $a = 190$ nm to ensure that the fundamental TE mode is resonant with the MoS₂ exciton ($\lambda_X = 660$ nm; λ_X is the photon wavelength in vacuum for frequency ω_X). Gallium phosphide is chosen as the material for the slab photonic crystal cavity, due to its high refractive index ($n = 3.2$) and transparency in that wavelength range. The choice of H1 cavity is primarily motivated by its small mode-volume ($\sim 0.45(\lambda_X/n)^3$) and mode area ($\sim (\lambda_X/n)^2$).

III. EFFECTIVE HAMILTONIAN AND POLARITON-POLARITON INTERACTION

In the uncoupled limit, photon is itinerant and exciton is localized. All interesting physics comes in when the light-matter interaction is turned on. In the regime when the light-matter interaction $\hbar\Omega$ is much greater than the photon hopping t [7], the many-body quantum dynamics close to the ground state is constrained to the lower-polariton Hilbert space and one can truncate the full Hamiltonian (1) into the following effective Hamiltonian [9]

$$\mathcal{H}_{pl} = -t_{pl} \sum_{\langle i,j \rangle} a_i^\dagger a_j + \frac{1}{2} \sum_i U_{pl} n_i (n_i - 1). \quad (4)$$

Here $t_{pl} = tp_c$ and $n_i = a_i^\dagger a_i$ with a_i^\dagger being polariton creation operator. $p_c \equiv \cos^2[\frac{1}{2}\text{arccot}(\frac{\Delta}{2\hbar\Omega})]$ is the photonic fraction of the lower polariton[9], where $\Delta \equiv \hbar(\omega_X - \omega_c)$ is the exciton-photon detuning. The polariton-polariton interaction U_{pl} is determined by the difference between the ground state energy of an isolated cavity with two quanta with and without

the exciton-exciton repulsion, respectively[7],

$$U_{pl} \equiv E_{GS}(2q) - E_{GS}^{(0)}(2q). \quad (5)$$

The ground state energy of the polaritonic system is calculated based on the following: The Hamiltonian of an isolated cavity with two energy quanta can be written in the basis of $(|2, 0\rangle, |1, 1\rangle, |0, 2\rangle)^T$ (here $|n_p, n_x\rangle$ with $n_p + n_x = 2$ are the Fock states with n_p photons and n_x excitons) as

$$\mathcal{H}_{2q} = \begin{pmatrix} 2\hbar\omega_c & \sqrt{2}\hbar\Omega & 0 \\ \sqrt{2}\hbar\Omega & \hbar(\omega_c + \omega_X) & \sqrt{2}\hbar\Omega \\ 0 & \sqrt{2}\hbar\Omega & 2\hbar\omega_X + U_X \end{pmatrix}. \quad (6)$$

The ground state of the above Hamiltonian consists of two interacting polaritons, of which the total energy is $E_{GS}(2q)$. When the interaction between exciton is turned off, $U_X = 0$, the ground state of the Hamiltonian gives two noninteracting polaritons, with total energy $E_{GS}^{(0)}(2q)$. The difference between the two energies of the ground states is the interaction energy between two polaritons within a cavity.

In the literature, there are two distinct regimes in which photon antibunching were observed and studied: (i) the photon blockade regime[21–24] where the QD size is small and thus $U_X \gg \hbar\Omega$, (ii) the polariton blockade regime[20] where the QD size is large and then $U_X \ll \hbar\Omega$. Photon blockade was observed experimentally in cavity-QD hybrid systems using small InAs QDs where the value of exciton-photon coupling strength is small, $\hbar\Omega \leq 0.16$ meV[24]. In these systems the polariton interaction U_{pl} is weak, $U_{pl} \leq 0.1$ meV[24].

One of the main conclusions in this paper is that the maximum polariton-polariton interaction is not reached in the photon blockade regime where the exciton-exciton repulsion is very strong, nor in the polariton blockade regime where the light-matter interaction is very strong. As illustrated in Fig. 1(b), the polariton-polariton interaction U_{pl} ramps up when the QD radius r_X is small (the photon blockade regime). After reaching to a maximum value around $r_X = 20$ nm, U_{pl} decays with the QD radius in the polariton blockade regime. The maximum value of U_{pl} lies in the crossover between the two regimes. To the best of our knowledge such non-monotonic behavior (also holds for other materials, see Supplementary Materials[26]) is never reported before. This finding indicates that there is an optimal QD radius for strong polariton-polariton interaction in each optoelectronic material.

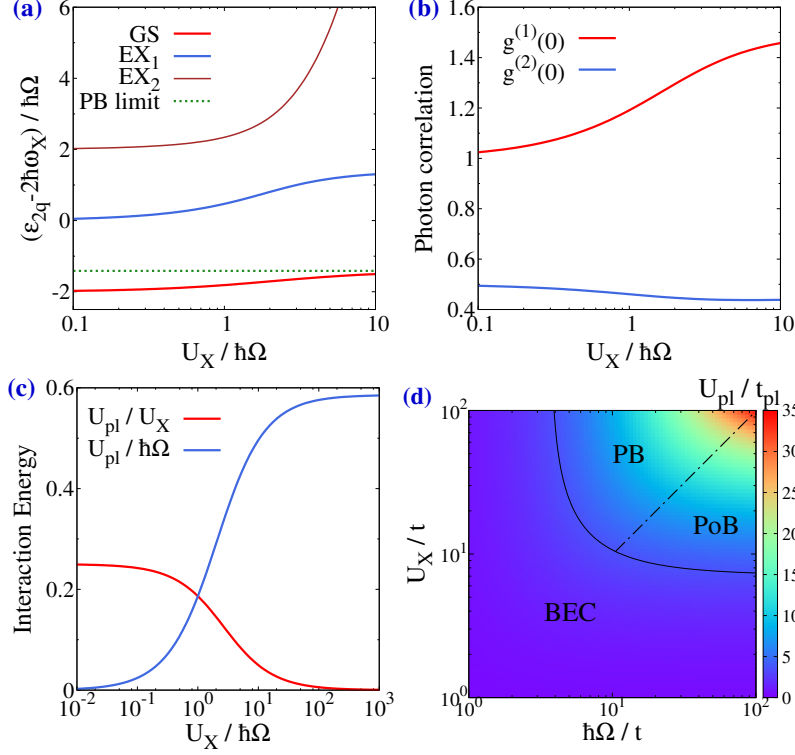


FIG. 2. Crossover from polariton blockade to photon blockade. (a) Energy levels ε_{2q} of the ground state (GS), the first and second excited states (EX₁ and EX₂) as functions of the exciton-exciton interaction U_X for a single cavity with two energy quanta. We scale the interaction energy U_X with the exciton-photon coupling $\hbar\Omega$. The dotted line denote the energy $-\sqrt{2}\hbar\Omega$, i.e., the GS energy in the photon blockade (PB) limit. (b) Photon correlation function $g^{(1)}(0)$ and $g^{(2)}(0)$ as functions of $U_X/(\hbar\Omega)$. (c) Polariton interaction energy U_{pl} for various $U_X/(\hbar\Omega)$. (d) α and phase diagram of 1D interacting polaritons with zero detuning. The Mott insulator phase consists two regions: the photon blockade (PB) region and the polariton blockade (PoB) region. The phase boundary between BEC and Mott insulator is labeled by the solid curve, while the crossover between PB and PoB regions is labeled by the chained curve.

To understand the underlying physics, we calculate the spectrum and photon correlation of the isolated cavity with two energy quanta. The energy levels of the Hamiltonian Eq.(6), denoted as ε_{2q} , as functions of the repulsive interaction U_X are given in Fig. 2(a). The photon blockade limit (i.e., when exciton repulsion U_X is much larger than the exciton-photon coupling $\hbar\Omega$) is represented by the dotted line. We find that the ground state energy $E_{GS}(2q)$ indeed increases with exciton-exciton repulsion U_X [see Fig. 2(a)] and the photon

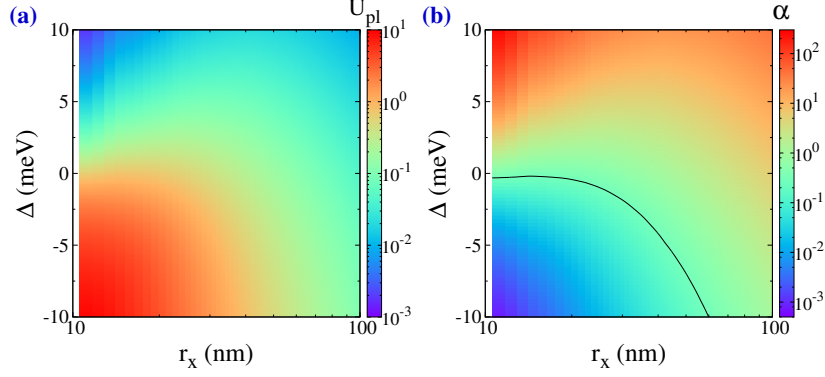


FIG. 3. (a) Polariton-polariton interaction U_{pl} vs. r_X and exciton-photon detuning Δ . (b) α and phase diagram for strongly interacting 1D polariton system for various MoS₂ QD radius r_X and exciton-photon detuning Δ with hopping energy $t = 0.5$ meV.

antibunching is stronger in the strong exciton repulsion regime [see Fig. 2(b)]. In this regime the first-order correlation function becomes greater than unity, as the manifestation of the projection out of the double exciton state [i.e., the 2nd excited state in Fig. 2(a)] due to strong exciton repulsion.

However, as shown in Fig. 1(b), strong exciton-exciton repulsion requires very small QD radius. Unfortunately for such small QD the light-matter interaction $\hbar\Omega$ is very small (due to much reduced overlap between the exciton and the photon field) and the polariton-polariton repulsive interaction is determined by $U_{pl} \simeq (2 - \sqrt{2})\hbar\Omega$ [see Fig. 2(c)]. Thus the polariton interaction U_{pl} is rather weakened with decreasing QD size in this regime, as indicated in Fig. 1(b).

In the other limit, when the light-matter interaction $\hbar\Omega$ is much stronger than the exciton-exciton repulsion U_X , the polariton interaction U_{pl} is limited by the exciton-exciton repulsion U_X [see Fig. 2(c)]. In this regime, increasing the QD size leads to greater light-matter interaction $\hbar\Omega$ but reduced exciton repulsion U_X (since $U_X = 6E_b a_B^2 / S_X$). Therefore, the polariton interaction U_{pl} decreases with increasing QD size. Following these reasonings, the non-monotonic dependence of the polariton-polariton interaction U_{pl} on the QD size shown in Fig. 1(b) is an universal behavior for all quantum-emitters. Indeed, we find that this behavior holds true for other common quantum emitters, such as GaAs, InAs, CdTe, GaN and MoSe₂ QDs. The optimal polariton-polariton interaction for all these quantum-emitters obtained from the parameters for the exciton and the light-matter interaction (i.e.,

d_{cv} , $|\phi(0)|$, L_c , E_b , and a_B) are listed in Table I, where the optimal QD radius ranging from several nanometers to tens of nanometers [see Supplementary Materials[26]]. We find that MoS₂ is one of the best material for strong polariton-polariton interaction. The other TMD material, MoSe₂, is also very appealing for quantum simulation. Further enhancement of the polariton-polariton repulsion can be achieved by engineering the cavity for stronger light trapping (i.e., smaller mode area to λ_X^2 ratio; λ_X is the photon wavelength in vacuum for frequency ω_X)

TABLE I. Optimal polariton-polariton interaction (in unit of meV) for quantum-emitters made of different materials in H1 cavity at zero exciton-photon detuning.

| Materials | MoS ₂ | MoSe ₂ | GaAs | InAs | GaN | CdTe |
|------------------|------------------|-------------------|------|------|------|------|
| Optimal U_{pl} | 0.85 | 0.48 | 0.32 | 0.16 | 0.51 | 0.33 |

We now illustrate the phase diagram of the 1D interacting polariton system at zero exciton-photon detuning in Fig. 2(d). The polariton Mott insulator phase exists in the region with *simultaneous* strong exciton-exciton interaction and strong exciton-photon interaction. The whole region can be separated into two regimes: the polariton-blockade regime and the photon-blockade regime. The crossover line (the dot-dashed line) is determined by $U_X = \hbar\Omega$. In the other regions the polariton-polariton interaction U_{pl} is not strong enough to drive the Mott transition, hence the system is in the BEC phase of polaritons. The Mott-BEC phase boundary is evaluated approximately via $\alpha = \alpha_c$ ($\alpha \equiv t_{pl}/U_{pl}$) with $\alpha_c = 0.28$ for filling factor $\nu = 1$ (i.e., one polariton per cavity)[30].

Using the material parameters of MoS₂ QD, we calculate the polariton-polariton interaction U_{pl} and the dimensionless parameter α for various detuning Δ and QD radius r_X [see Figs. 3(a) and 3(b)]. The polariton-polariton interaction can be greater than 1 meV for MoS₂ for negative detuning. However, at too large negative detuning, the polaritons behave like an exciton, and impedes photonic quantum simulation as the photon addressability of the polaritons is significantly reduced. From Fig. 3(a) the accessible polariton repulsion can be as large as several meV. The dimensionless parameter α gives the parameter regimes for polariton Mott insulator, where the phase boundary is evaluated again via $\alpha = \alpha_c$ as indicated by the black curve.

To confirm the above findings, we performed full quantum optical simulation of a tuned

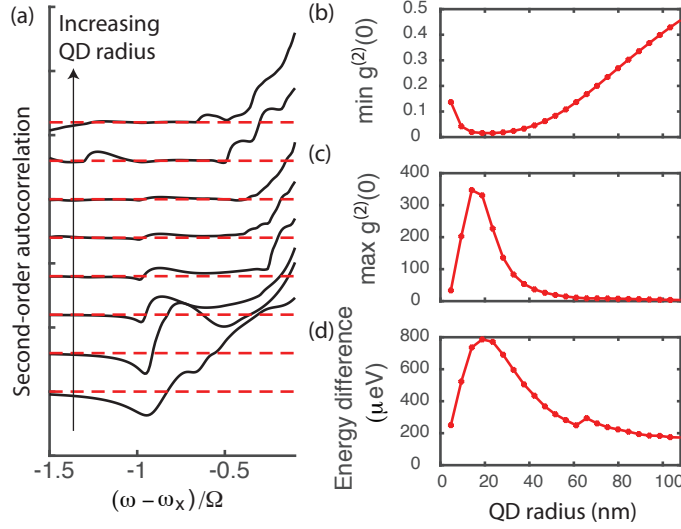


FIG. 4. (a) Second-order autocorrelation $g^{(2)}(0)$ vs. optical frequency ω for various QD radius for a MoS₂ QD in a single cavity as calculated using the Lindblad formalism. The correlation function $g^{(2)}(0)$ has a dip (antibunching) at the lower-polariton frequency, $\omega_X - \Omega$, and a peak (bunching) on the high-frequency shoulder close to the dip. (b) The minimum $g^{(2)}(0)$ at the dip, (c) the maximum $g^{(2)}(0)$ on the high-frequency shoulder vs. the QD radius as extracted from (a). (d) The frequency difference (as converted to energy difference) between the dip and the peak vs. the QD radius. The detuning of the quantum emitter and the photon cavity is $\Delta = 0$.

single H1-cavity—MoS₂-QD hybrid structure, in presence of the excitonic and photonic losses. In our simulations, the excitonic loss rate γ_X and photonic loss rate γ_c are assumed to be same ($\gamma_X = \gamma_c = 2\pi$ GHz). We numerically calculate the evolution of the density matrix by using the standard Lindblad formalism [31, 32]. The calculated second-order correlation function $g^{(2)}(0)$ shows that the photon-antibunching takes place at the lower-polariton frequency $\omega = \omega_X - \Omega$, corresponding to a dip in the autocorrelation function $g^{(2)}(0)$ [see Figs. 4(a) and 4(b)]. This is consistent with both the pictures of photon blockade and polariton blockade. On the high-frequency shoulder close to the dip, there always exists a peak of the second-order correlation $g^{(2)}(0)$ [see Figs. 4(a) and 4(c)]. This photon bunching corresponds to the resonant excitation of double occupancy of interacting polaritons (i.e., adding another polariton to a cavity that already has one polariton). Therefore, the frequency difference between the peak and the dip, $\omega_{peak} - \omega_{dip} = \omega_{peak} - \omega_X + \Omega \simeq U_{pl}/\hbar$,

gives a good evaluation of the polariton interaction strength U_{pl} . This frequency difference is indeed maximized for the QD radius slightly below 20 nm [see Fig. 4(d)]. Both the photon antibunching at the dip and the bunching at the peak become very significant for that optimized QD radius [see Figs. 4(b) and 4(c)].

IV. QUANTUM MANY-BODY SIMULATION IN A FINITE CHAIN OF COUPLED CAVITIES

The effect of strong interaction between polaritons can be characterized by the second- and third- order correlation functions which can be measured experimentally[12]. We have studied such correlation functions for single cavities in the previous sections. We now show that these correlations can also extract useful information of the complex many-body ground state wavefunction of a finite 1D chain of serially coupled cavities.

We calculate the ground state wavefunction of a 1D lattice of interacting polaritons using exact diagonalization method. We use periodic boundary condition for $N = 10$ sites where each site can have maximum 3 polaritons. We note that for a chain of cavities, we did not consider loss, as a full master equation simulation of the whole chain is computationally intractable due to extremely large Hilbert space. While this is a limitation of the present theoretical treatment, it is the same reason why quantum simulation is highly sought after. The ground state wavefunction of the system is very complex. It contains many kinds of long-range multi-particle entanglement[13]. A way to characterize such entanglement is to measure the multi-photon correlations. We calculate the following correlation functions using the many-body *ground state* obtained from exact diagonalization of the Bose-Hubbard Hamiltonian (4):

$$g_{ij}^{(2)}(0) = \frac{\langle a_i^\dagger a_j^\dagger a_i a_j \rangle}{\langle a_i^\dagger a_i \rangle \langle a_j^\dagger a_j \rangle}, \quad (7)$$

$$g_{i \neq j \neq l}^{(3)}(0) = \frac{\langle n_i n_j n_l \rangle}{\langle n_i \rangle \langle n_j \rangle \langle n_l \rangle}, \quad (8)$$

where $n_i = a_i^\dagger a_i$. In the regime where $\hbar\Omega \gg t$ the lower polariton picture is well-defined, the $g_{ij}^{(2)}(0)$ correlation function is proportional to the second-order photon correlation that can be determined via Hanbury Brown and Twiss measurements. We calculate $g^{(2)}(0)$ and $g^{(3)}(0)$ for the ground state with various U_{pl}/t_{pl} (results are shown in Figs. 5(a) and 5(b)). The second-

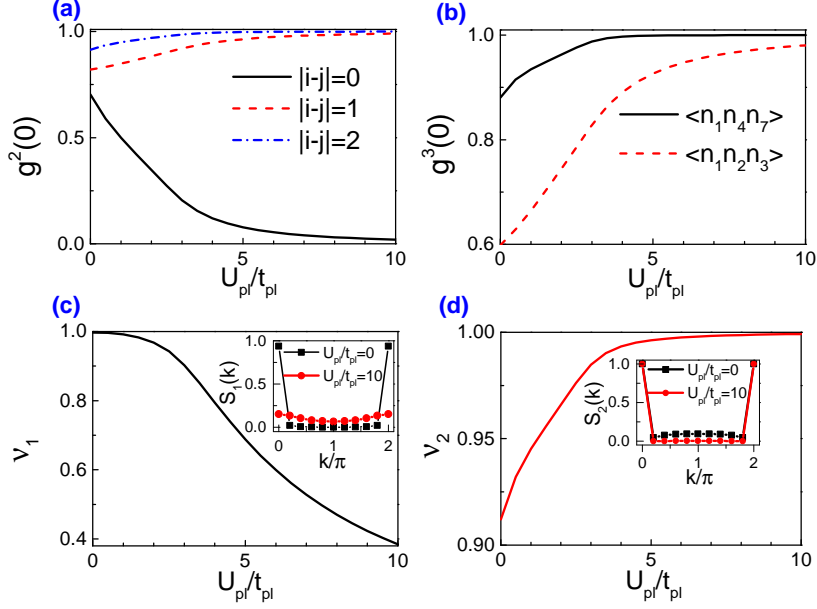


FIG. 5. Second-order and third-order correlation function of the ground state of 1D Bose-Hubbard model Eq. (4). (a) Equal-time second-order correlation functions $g^{(2)}(0)$ at the same site (black curve) and for nearby sites (red and blue curves) vs. U_{pl}/t_{pl} . (b) Equal-time third-order correlations for nearby sites as functions of U_{pl}/t_{pl} . (c) The structure factor $S_1(k)$ for photon field and visibility fringe \mathcal{V}_1 for different U_{pl}/t_{pl} . (d) The structure factor $S_2(k)$ for photon number and visibility fringe \mathcal{V}_2 for various U_{pl}/t_{pl} .

order correlation function at the same site $g_{ii}^{(2)}(0)$ decreases quickly with increasing U_{pl}/t_{pl} , which signifies photon antibunching due to strong polariton repulsion. On the other hand $g^{(2)}(0)$ at different sites increases with increasing U_{pl}/t_{pl} , consistent with the understanding that the Mott insulator state is mostly a product state (plus quantum fluctuations) with each site occupied by a single polariton. Fig.5(b) shows the build-up of $g^{(3)}(0)$ correlations with increasing U_{pl}/t_{pl} which signifies the localization of polaritons due to their mutual repulsion. Those correlation functions reveal the complex inter-particle entanglement in the strongly interacting polariton systems which can be sources for nonclassical, highly-entangled light.

We also computed the following structure factors

$$S_1(k) = \frac{1}{N} \sum_j \langle a_i^\dagger a_j \rangle e^{ik(i-j)/N}, \quad (9)$$

$$S_2(k) = \frac{1}{N} \sum_j \langle n_i n_j \rangle e^{ik(i-j)/N}, \quad (10)$$

as well as the visibility fringes[5–7]

$$\mathcal{V}_1 = \frac{S_1|_{max} - S_1|_{min}}{S_1|_{max} + S_1|_{min}}, \quad (11)$$

$$\mathcal{V}_2 = \frac{S_2|_{max} - S_2|_{min}}{S_2|_{max} + S_2|_{min}}. \quad (12)$$

The results are plotted in Figs. 4(c) and 4(d). The visibility fringe \mathcal{V}_1 decreases dramatically with increasing U_{pl}/t_{pl} , which is the signature of the emergence of the Mott insulator state. On the other hand, the visibility fringe \mathcal{V}_2 increases only slightly with increasing U_{pl}/t_{pl} . The visibility fringe \mathcal{V}_1 has large contrast for the BEC and Mott insulator states because the BEC is a coherent state with long range single-particle correlation, while the Mott insulator is a gapped state with short-range single-particle correlation.

V. QUANTUM SIMULATION OF SUPERLATTICES OF COUPLED CAVITY ARRAYS

We now introduce a method for quantum simulation of superlattices of serially coupled cavity arrays. This can be done via modulating the detuning, for example, by making the detuning at even (odd) lattice sites as $\Delta(-\Delta)$. The opposite detunings at two cavities modify the single particle spectrum and the effect of interaction. The single particle spectrum of a pair of such detuned cavities is plotted in Fig. 6(a). The splitting between the ground state and the first excited state is $\sqrt{\Delta^2 + t^2}$. Thus at large detuning $|\Delta|$ the full Hamiltonian can be truncated into the Hilbert space of the lowest energy state of a pair of cavity. In this regime each pair of cavities contribute only one single particle state (see Fig. 6(b)). Therefore, at half-filling $\nu = 1/2$ the polaritons system can have phase transition into the Mott insulator state if the interaction between polaritons is strong.

We calculate the many-body ground state of a finite chain of coupled cavities (with 10 cavities) for filling factor $\nu = 1/2$ and $\nu = 1$ by exact diagonalization of the many-body Hamiltonian with a cut-off of the single site Hilbert space at three bosons. From the ground

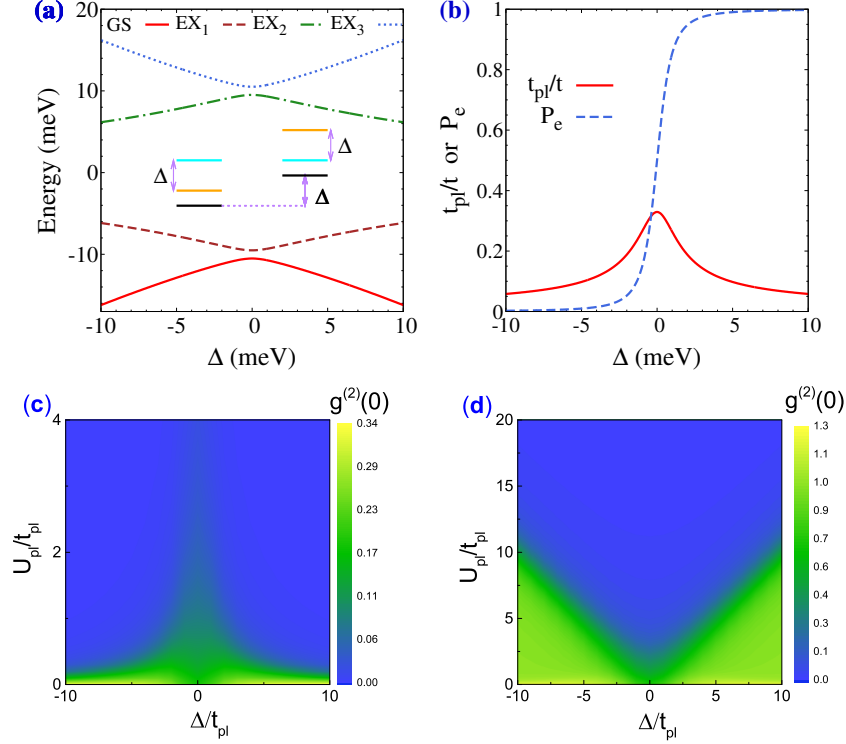


FIG. 6. Quantum simulation in 1D Cavity-QD superlattices. (a) Single-particle energy spectrum of coupled double cavity. Inset: Left (right) is the exciton (cyan), cavity (orange), lower polariton (black) energy levels for the even (odd) sites. The detuning at the even sites is positive, while at the odd sites it is negative. The energy difference between lower polariton levels in the two different sites is just the detuning Δ . (b) Hopping energy t_{pl}/t and the probability at even site P_e as functions of the detuning. Parameters for (a) and (b): $t = 1$ meV and $\hbar\Omega = 10$ meV. (c) The correlation function $g^{(2)}(0)$ (averaged over the odd and even sites) as a function of the staggered detuning and the interaction strength for filling factor $\nu = 1/2$ in a finite chain of 10 sites. (d) Similar to (c) but with filling factor $\nu = 1$.

state wavefunction, we can obtain the second-order correlation function $g^{(2)}(0)$ for the even sites and the odd sites. The averaged $g^{(2)}(0)$ is more relevant to experimental measurements since it is difficult to distinguish photons from the even site or the odd site. The significant reduction of the $g^{(2)}(0)$ correlation function below unity signifies the transition into the Mott insulator states. For half-filling, the Mott transition is facilitated by the staggered detuning, which is consistent with the superlattice picture. For $\nu = 1$ filling, the effective filling factor at large detuning $|\Delta|$ is 2. Since the Mott transition at higher filling factor requires larger

interaction strength, the staggered detuning impedes Mott transition in the large detuning $|\Delta|$ regime for $\nu = 1$. Our numerical simulation is also inconsistent with a few-particle analysis in the Supplemental Materials.

VI. REALISTIC CONSIDERATIONS ON EXPERIMENTAL REALIZATION

It is known that lack of control over self-assembled QDs positioning thwarts the scalability of the nonlinear polariton system. Deterministic fabrication and positioning of the QDs, by patterning a quantum well like structure can potentially solve this problem. Unfortunately, such patterning of usual quantum wells degrades the exciton significantly[33]. Monolayer materials have been proven to be chemically and mechanically stable and robust[34–36], and can potentially circumvent these problems of usual optoelectronic materials.

The difficulties in precisely positioning QDs to the center of each cavity are due to incompatibility of the fabrication method of photonic crystal cavity and that of the QD. Recently new fabrication methods for MoS₂ monolayer QDs was developed where size and position of QDs can be controlled much more precisely than previous methods using lithography[37]. The main advantages of using MoS₂ monolayer QDs is its unique material compatibility, and robustness against etching (due to its mechanical and chemical stability)[38]. Recent works have demonstrated growth of a large area of monolayer material[39]. In practice one can start with such a large area of monolayer materials, and pattern it to create an array of quantum dots. The current state-of-the-art electron-beam technology can fabricate structure reliably with sub-1 nm accuracy. A significant uncertainty comes from the etching process, as the lateral etching of the structure is probabilistic, and creates large non-uniformity. However, delicate fabrication with electron-beam lithography and etching of photonic crystal cavities showed an uncertainty of only 10 nm. Monolayer materials provide an excellent opportunity, because due to the thinness of the material, etching them is simple, and does not cause large lateral etching that degrades the quality of the sample. Hence, fabricating 20 nm radius quantum dot, and patterning them in an array with periodicity of ~ 200 nm is well within the current fabrication capability. In the experiment, one can first fabricate the coupled cavity array, and then transfer the 2D material to the photonic chip. One can perform an overlay to align the monolayer quantum dots with the cavities. Note that, current electron-beam technology also provides an overlay accuracy of

1 nm. As the cavity lateral mode size is significantly bigger than 1 nm, the fluctuation in exciton-photon coupling due to QD positioning can be effectively suppressed. Since the etching processes affect the photonic crystal cavity negligibly, this method also decouples the correlation between various parameters in our model.

The main dissipation mechanisms in the coupled-cavity-array system come from the finite exciton and photon lifetimes[14]. The state-of-art fabrication technology of photonic crystal cavity has enabled good control of cavity frequency and very high quality factors (over 1 million)[40]. With such fabrication technology, one can have good control of cavity resonance with wavelength uncertainty below 1 nm[40]. The finite lifetime due to exciton non-radiative decay is, however, a major challenge. Note that recent works have demonstrated good surface passivation to reduce the non-radiative recombination[41]. These experimental advancement encourages us to believe that the exciton nonradiative decay in the QDs can be as long as the exciton lifetime in the monolayer ($\gtrsim 70$ ps). At sub-1 K temperature, exciton nonradiative decay is further suppressed, which is negligible as the resulting exciton linewidth is much smaller than other energy scales such as t_{pl} and U_{pl} (~ 1 meV).

VII. CONCLUSION AND DISCUSSIONS

We propose to realize strongly interacting polariton systems based on MoS₂ QD coupled with the H1 photonic crystal cavity. The material design enables simultaneous realization of strong exciton-photon coupling and strong exciton-exciton repulsion. This advantage results in polariton interaction one order of magnitude stronger than in the state-of-art single-photon quantum optical systems. The strongly interacting polariton systems can serve as a platform for quantum simulation of many-body entanglement and dynamics at the energy scale of meV and light sources of highly-entangled, non-classical photons. We discovered that the optimal polariton interaction is realized near the crossover between photon blockade and polariton blockade for single-QD in each cavity.

The fluctuation effects may cause difficulties in realization of quantum phase transition from BEC to Mott insulator. On the other hand, it was shown that fluctuations in coupled cavity systems can lead to polaritonic glass phases[7]. The interplay between disorder and interaction effects in localization of bosonic particles is an interesting physics problem that has been studied for a long time but unsolved. This regime is also related to many-body lo-

calization which is an area gaining significant attention recently[42]. In the other limit, even a few coupled cavities [38] can provide a platform for quantum simulation of strongly interacting few-particle bosonic systems and serve as multi-photon entanglement light sources[43]. Finally, we remark that recent experiments have shown that exciton-exciton interaction can be tuned via the density of coexisting electrons (or holes) in the QDs[44], offering additional tunability of the system.

ACKNOWLEDGMENTS

H.X.W and J.H.J acknowledge supports from National Natural Science Foundation of China (grant no. 11675116) and the Soochow University. J.H.J also thanks Sajeev John, Gang Chen, and Ming-Qi Weng for helpful discussions. A.Z and A.M are supported by the National Science Foundation under grant NSF-EFRI-1433496; and the Air Force Office of Scientific Research-Young Investigator Program under grant FA9550-15-1-0150. A.M. also acknowledges useful discussions with Xiaodong Xu. W.L.Y acknowledges support by the Natural Science Foundation of Jiangsu Province of China under Grant No. BK20141190 and the National Science Foundation of China under Grant No. 11474211. Y.D.X and H.Y.C thank supports from the National Science Foundation of China for Excellent Young Scientists (no. 61322504).

-
- [1] K. Kang et. al., *Nature (London)* **520**, 656 (2015).
 - [2] M. Greiner, O.Mandel, T. Esslinger, T. W. Hansch, and I. Bloch, *Nature (London)* **415**, 39 (2002).
 - [3] I. Bloch, J. Dalibard, and S. Nascimbene, *Nature Phys.* **8**, 267 (2012).
 - [4] D. E. Chang, V.Vuletić, and M. D. Lukin, *Nat. Photon.* **8**, 685 (2014).
 - [5] M. J. Hartmann, F. G. S. L. Brand ao, and M. B. Plenio, *Nature Phys.* **2**, 849 (2006).
 - [6] D. G. Angelakis, M. F. Santos, and S. Bose, *Phys. Rev. A.* **76**, 031805(R) (2007).
 - [7] D. Rossini and R. Fazio, *Phys. Rev. Lett.* **99**, 186401 (2007).
 - [8] C. Noh and D. G. Angelakis, *Rep. Prog. Phys.* **80**, 016401 (2016).
 - [9] I. Carusotto and C. Ciuti, *Rev. Mod. Phys.* **85**, 299 (2013).

- [10] S. Buckley, K. Rivoire, and J. Vučković, Rep. Prog. Phys. **75**, 126503 (2012).
- [11] T. Byrnes, N. Y. Kim, and Y. Yamamoto, Nature Phys. **10**, 803 (2014).
- [12] A. Rundquist *et al.*, Phys. Rev. A **90**, 023846 (2014).
- [13] X. G. Wen, *Quantum Field Theory of Many-Body Systems* (Oxford University Press, 2004).
- [14] J.-H. Jiang and S. John, Phys. Rev. X **4**, 031025 (2014).
- [15] J. Kasprzak *et al.*, Nature (London) **443**, 409 (2006).
- [16] R. Balili, V. Hartwell, D. Snoko, L. Pfeiffer, and K. West, Science **316**, 1007 (2007).
- [17] J. H. Jiang and S. John, Sci. Rep. **4**, 7432 (2014).
- [18] H. S. Nguyen *et al.*, Phys. Rev. Lett. **110**, 236601 (2013).
- [19] D. Ballarini *et al.*, Nat. Commun. **4**, 1778 (2013).
- [20] A. Verger, C. Ciuti, and I. Carusotto, Phys. Rev. B **73**, 193306 (2006).
- [21] K. M. Birnbaum, A. Boca, R. Miller, A. D. Boozer, T. E. Northup, and H. J. Kimble, Nature (London) **436**, 87 (2005).
- [22] A. Faraon, I. Fushman, D. Englund, N. Stoltz, P. Petroff, and J. Vučković, Nature Phys. **4**, 859 (2008).
- [23] A. Reinhard, T. Volz, M. Winger, A. Badolato, K. J. Hennessy, E. L. Hu, and A. Imamoglu, Nat. Photon. **6**, 93 (2012).
- [24] K. Müller *et al.*, Phys. Rev. Lett. **114**, 233601 (2015).
- [25] J. Hagemeyer *et al.*, Opt. Exp. **20**, 24714 (2012).
- [26] See Supplementary Materials, <http://>
- [27] S. Dufferwiel *et al.*, Nat. Commun. **6**, 8579 (2015).
- [28] D. Y. Qiu, F. H. da Jornada, and S. G. Louie, Phys. Rev. Lett. **111**, 216805 (2013).
- [29] F. Tassone and Y. Yamamoto, Phys. Rev. B **59**, 10830 (1999).
- [30] T. D. Kühner and H. Monien, Phys. Rev. B **58**, R14741(R) (1998).
- [31] A. Majumdar *et al.*, Phys. Rev. B **84**, 085309 (2011).
- [32] C. Gardiner and P. Zoller, *Quantum Noise*, 3rd ed. (Springer, Berlin, 2004).
- [33] T. C. Weisbuch, R. Dingle, A.C. Gossard, and W. Wiegmann, Solid State Comm. **38**, 709-712 (1981).
- [34] K. F. Mak, C. Lee, J. Hone, J. Shan, and T. F. Heinz, Phys. Rev. Lett. **105**, 136805 (2010).
- [35] Q. H. Wang, K. Kalantar-Zadeh, A. Kis, J. N. Coleman, and M. S. Strano, Nat. Nanotech. **7**, 699 (2012).

- [36] X. Xu, W. Yao, D. Xiao, and T. F. Heinz, *Nature Phys.* **10**, 343 (2014).
- [37] G. Wei *et al.*, arXiv: 1510.09135.
- [38] S. Wu *et al.*, *Nature (London)* **520**, 69 (2015).
- [39] D. Dumcenco *et al.*, *ACS Nano*, **9**, 4611 (2015).
- [40] S. Noda, M. Fujita, and T. Asano, *Nat. Photon.* **1**, 449 (2007).
- [41] M. Amani *et al.*, *Science* **350**, 1065 (2015).
- [42] V. Oganesyan and D.A. Huse, *Phys. Rev. B* **75**, 155111 (2007); A. Pal and D.A. Huse, *Phys. Rev. B* **82**, 174411 (2010); Ehud Altman and Ronen Vosk, *Ann. Rev. Cond. Matt. Phys.* **6**, 383 (2015).
- [43] J.-W. Pan, Z.-B. Chen, C.-Y. Lu, H. Weinfurter, A. Zeilinger, and M. Zukowski, *Rev. Mod. Phys.* **84**, 777 (2012).
- [44] M. Sidler *et al.*, arXiv:1603.09215